



IMPACT OF WAKE MODELING UNCERTAINTY ON HELICOPTER ROTOR AEROACOUSTIC ANALYSIS

Stavros Vouros, Ioannis Goulos, Calum Scullion, Devaiah Nalianda and Vassilios Pachidis

Centre for Propulsion Engineering, School of Aerospace Transport and Manufacturing
Cranfield University, Bedfordshire, MK43 0AL, UK

Corresponding and lead author; e-mail address: s.vouros@cranfield.ac.uk

ABSTRACT

Free-wake models are routinely used in aeroacoustic analysis of helicopter rotors; however, their semi-empiricism is essentially accompanied with uncertainty related to physical wake parameters. In some cases, analysts have to resort to empirical adaption of these parameters based on previous experimental evidence. This paper investigates the impact of inherent uncertainty in wake aerodynamic modeling on the robustness of helicopter rotor aeroacoustic analysis. A free-wake aeroelastic rotor model is employed to predict high-resolution unsteady airloads, including blade-vortex interactions. A rotor aeroacoustics model, fundamentally based on Acoustic Analogy, is utilized to calculate aerodynamic noise in the time-domain. The individual analytical models are incorporated into a stochastic analysis numerical procedure, implemented through non-intrusive Polynomial Chaos expansion. The possible sources of uncertainty in wake tip-vortex core modeling are identified and their impact on noise predictions quantified. When experimental data to adjust the tip-vortex core model are not available the uncertainty in acoustic pressure and ground noise impact at observers dominated by blade-vortex interaction noise can reach up to 25% and 3.50 dB respectively. This work aims to devise generalized uncertainty maps to be used as modeling guidelines for aeroacoustic analysis in the absence of the robust evidence necessary for calibration of semi-empirical vortex core models.

NOMENCLATURE

Roman Symbols

a	Lower limit of uniform distribution	
A_{cs}	Blade element cross sectional area	m^2
b	Upper limit of uniform distribution	
c_0	Speed of sound	m/s
c_b	Blade chord	m
C_L	Rotor disc rolling moment coefficient $= L / (\rho \pi \Omega^2 R^5)$	
C_M	Rotor disc pitching coefficient $= M / (\rho \pi \Omega^2 R^5)$	
$C_n M^2$	Normal force coefficient $= F_n / (0.5 \rho c_0^2 c_b)$	
C_T	Rotor disc thrust coefficient $= T / (\rho \pi \Omega^2 R^4)$	
COV	Coefficient of variation $= \mu / \sigma$	
d	Perpendicular distance between a point and a vortex filament	m
dy	Blade differential span length	m
$f = 0$	Acoustic data line function	
F_n	Sectional normal force	N/m
\vec{l}_{12}	Vortex filament vector	m
\vec{L}	Blade sectional loading vector	N/m
L	Rotor rolling moment	Nm
\vec{M}	Relative Mach number vector	
$ \vec{M} $	Magnitude of relative Mach number	
M	Rotor pitching moment	Nm
Mo	Mode of distribution	
n	Number of uncertain input parameters	

$N_{Pearson}$

$N_{Pearson}$	Pearson's correlation index	
$OASPL$	Overall Sound Pressure Level	dB
P	Order of polynomial expansion	
p'	Acoustic pressure	Pa
p'_m	Monopole acoustic pressure	Pa
p'_d	Dipole acoustic pressure	Pa
\vec{r}	Position vector of a point on a vortex filament	m
\hat{r}	Unit radiation vector	
r	Radiation distance	m
r_c	Tip vortex viscous core radius	m
r_{c0}	Initial tip vortex viscous core radius	m
\vec{r}_1	Position vector of a point relative to the beginning of a vortex filament	m
\vec{r}_2	Position vector of a point relative to the end of a vortex filament	m
R	Rotor radius	m
$R(n, m)$	Shorthand notation function	m^{-n}
S_i	Sobol sensitivity index	
t	Observer time	s
T	Rotor thrust	N
\vec{V}_{ind}	Induced velocity vector	m/s
W	Shorthand notation term	m/s
\vec{x}	Observer position vector, with components x_i	m
y	Stochastic response of system at specific collocation point	
Y	Stochastic response of system	

Greek Symbols

α	Oseen constant for the vortex core radius
----------	---

α_1	Squire parameter for the eddy viscosity factor	
a_i	Coefficient of orthogonal polynomial basis function	
α_s	Wind tunnel rotor shaft angle	rad
Γ	Circulation	m ² /s
γ_1	Skewness of distribution	
γ_2	Excess kurtosis of distribution	
δ	Eddy viscosity parameter	
ζ	Distance along trailed tip vortex	rad
μ	Mean value of distribution	
ν	Kinematic viscosity	m ² /s
ξ	Distribution	
ρ_0	Density of quiescent medium	kg/m ³
σ	Standard deviation of distribution	
φ_i	Polynomial basis function	
ψ	Blade azimuthal position	rad
Ω	Rotor rotational speed	rad/s

Subscripts

$(\cdot)_{amp}$	Amplitude
-----------------	-----------

Superscripts

$(\cdot)^{adv}$	Quantity referring to rotor advancing side
$(\cdot)^{inflow}$	Vortex core quantity used to evaluate induced velocity for inflow calculations
$(\cdot)^{ret}$	Quantity referring to rotor retreating side
$(\cdot)^{wake}$	Vortex core quantity used to evaluate induced velocity for wake calculations

1. INTRODUCTION

Helicopter noise prediction is essentially affiliated with the aerodynamic modeling of the rotor flowfield (Ref. [1]). Free-wake aerodynamic modeling methods are capable of efficiently predicting complex aerodynamic phenomena like blade-vortex interactions (BVI), through detailed resolution of rotor wake behavior (Ref. [2]). The aforementioned models require some user-defined input parameters related to rotor wake physics. These parameters are typically obtained from experiments or empiricism; hence they are effectively associated with inherent uncertainty which is propagated in the prediction of rotor aeroacoustics. The identification of wake aerodynamic sources of uncertainty and quantification of their impact on aeroacoustic predictions are deemed as indispensable towards the design, certification and operation of present and future rotorcraft.

The majority of aeroacoustic uncertainty investigations to date have predominantly focused on geometrical and operational input uncertainties. In Ref. [3] a benchmark rod-airfoil configuration was assessed in terms of geometric uncertainty and its propagation in aeroacoustics. A Large-Eddy Simulation (LES) solver

was coupled with an aeroacoustic solver within a non-intrusive stochastic collocation method (Ref. [4]). It was shown that an uncertainty of ± 0.004 m in the position of the rod led to an uncertainty of 0.5-1 dB in the Overall Sound Pressure Levels (OASPL) (Ref. [3]).

Olsman (Ref. [5]) quantified the uncertainty associated with ground acoustic footprint of noise abatement flight procedures in the presence of randomness in the operational flight path. A noise hemisphere approach was employed for the prediction of noise footprint and incorporated into a Polynomial Chaos expansion (PCE) based framework for uncertainty quantification. Standard deviations of up to 3 dB were calculated with respect to the deterministic solution, which dictate the potential importance of stochastic noise footprint prediction in helicopter mission planning.

Ricks *et al.* (Refs. [6], [7]) investigated the impact of operational and geometrical uncertainty in the acoustic propagation stage of hybrid computational aeroacoustics. A Computational Fluid Dynamics (CFD) solver based on the inviscid Euler equations was coupled with an integral solution of the noise propagation equation for the prediction of noise generation and propagation. A non-lifting helicopter rotor in hover was considered and an in-plane noise observer located 3.09 rotor radii upstream of the rotor. PCE was employed for the quantification of uncertainty and sensitivity analysis using Sobol indices. Uncertainty of 7.36% was observed in the peak acoustic pressure, primarily attributed to the randomness in blade tip Mach number. The investigations of this study were carried out for in-plane observers, dominated by thickness noise.

Gennaretti *et al.* (Ref. [2]) assessed the capabilities of a boundary-element-based computational methodology as regards BVI noise prediction. The study included a sensitivity analysis which showed that the wake model is sensitive to vortex core diffusion empirical coefficients. The analysis was a sensitivity investigation, based on the assumption of $\pm 50\%$ variation of wake diffusion parameters.

Bhagwat and Ramasamy (Ref. [8]) examined the effect of tip-vortex aperiodicity on the measurement uncertainty of vortex-core properties. Uncertainties in the order of 10% were calculated for the vortex core radius of the HART II rotor (Ref. [9]) in BVI conditions. These levels of uncertainty are representative of the state-of-the-art in tip-vortex measurements, although they have never been incorporated into helicopter rotor aeroacoustic simulation. In some cases, robust experimental evidence referring to tip-vortex core radius is not available, forcing analysts to resort to empiricism for the determination of the associated physical properties necessary for aerodynamic calculations.

The vortex core radius is a critical aerodynamic parameter which affects airloads and consequently, noise. To the authors' knowledge, the impact of tip-vortex core modeling uncertainty on the robustness of aeroacoustic predictions has not yet been systematically investigated. The general scope of this work is the quantification of the impact of wake modeling uncertainty on helicopter rotor BVI noise predictions. Furthermore, it is aimed to devise a set of fundamental modeling guidelines applicable when uncertainty is present in the governing wake tip-vortex

core physical parameters.

2. MATHEMATICAL FORMULATION

2.1. Aeroelastic rotor model

A free-wake and unsteady aeroelastic rotor model is utilized to predict elastic rotor blade unsteady motion and unsteady airloads, including BVIs (Ref. [10]). A minimum potential energy method, similar to the one reported in Ref. [11], is deployed for the estimation of coupled flap-lag-torsion vibration characteristics of the elastic rotor blades (Ref. [12]). The matrix/vector based formulation presented in Ref. [13] is employed for modeling the flexible rotor blade kinematics along with the Leishman-Beddoes indicial response method (Ref. [14]) for the prediction of unsteady blade airloads. The aforementioned models have been extensively described in the corresponding references; thus, further discussion will be omitted.

A relaxation-type free-wake aerodynamic model is employed for the modeling of unsteady rotor inflow, able to capture the complex blade-vortex interaction phenomena (Ref. [15]). Each vortex is discretized as a series of straight vortex filaments with Lagrangian markers located at the ends of each filament. It is assumed that viscous effects are significant only within the vortex core region of the filaments. Subsequently, the flow can be considered as inviscid outside the vortex singularity (Ref. [16]). The governing equation which describes the convection of the Lagrangian markers is the unsteady Vorticity Transport Equation for incompressible and isotropic fluids (Ref. [16]).

The velocity induced by a single vortex filament is evaluated through numerical integration using the Biot-Savart law for straight vortex filaments including the Vatisstas vortex core model (Ref. [17]):

$$\vec{V}_{ind} = \frac{\Gamma}{4\pi} \left(\frac{d}{(r_c^{2n} + d^{2n})^{1/n}} \right) \frac{\vec{l}_{12}}{|\vec{l}_{12}|} \cdot \left(\frac{\vec{r}_1}{|\vec{r}_1|} - \frac{\vec{r}_2}{|\vec{r}_2|} \right) \cdot \left(\frac{\vec{l}_{12} \times \vec{r}}{|\vec{l}_{12} \times \vec{r}_1|} \right) \quad (1)$$

where Γ is the circulation strength of the vortex, \vec{l}_{12} is the vortex filament vector, \vec{r}_1 and \vec{r}_2 are the position vectors of the arbitrary point P relative to the Lagrangian markers of the filament and \vec{r} is the position vector of point P relative to the vortex segment. The perpendicular distance between point P and the vortex filament is $d = |\vec{l}_{12} \times \vec{r}| / |\vec{l}_{12}|$. The tangential velocity profile of the Vatisstas model is defined by the general constant n which best matches the experimental velocities measured in Ref. [17]. Finally, the vortex core radius r_c is given by Squire's equation:

$$r_c(\zeta) = \sqrt{r_{c0}^2 + 4\alpha\delta\nu \frac{\zeta}{\Omega}} \quad (2)$$

where r_{c0} is the initial core radius and $\alpha = 1.25643$ is the Oseen constant. The eddy viscosity parameter δ is calculated by:

$$(3) \quad \delta = 1 + \alpha_1 \frac{\Gamma}{\nu}$$

Bhagwat *et al.* (Ref. [18]) suggested values in the order of 10^{-4} to 10^{-3} for the Squire parameter α_1 to represent viscous core growth of small scale rotors. Although the initial vortex core radius of 5-10% chord is typically used for forward flight, a larger initial core radius $r_{c0} = 0.6c$ has been used in some studies to reduce spurious BVI response in descending flight (Ref. [9]). Different core radii may be used for the evaluation of induced velocity for wake calculations and rotor inflow calculations, to improve convergence stability and speed (Ref. [9]). For the present analysis, the reference values of $r_{c0}^{wake} = 0.1c$ and $a_1^{wake} = 0.001$ are used for wake calculations, and $r_{c0}^{inflow} = 0.6c$ and $a_1^{inflow} = 0.008$ for rotor inflow calculations. These values provide the best match between predicted and measured wake, airloads and noise data. These values will serve as mean values for the uncertainty analysis, with appropriately chosen statistical distributions around them. This will be further discussed in Section 3.2.

The wake is split in the near wake and far wake regions which are linked via a vortex roll-up model based on the distribution of bound circulation and local vorticity $\partial\Gamma(r)/\partial r$. The rotor azimuthal step implemented is $\Delta\psi = 1 \text{ deg.}$ to efficiently capture the BVI airloads. The blades are discretized into 30 radial elements and six vibration modes are considered. The aforementioned resolutions have been selected after sensitivity analyses and literature suggestions (Ref. [16]). Shed vortices are not resolved in the wake model as they are fundamentally accounted for in the unsteady blade aerodynamic model through the deficiency functions applied on the circulatory normal force coefficient (Ref. [14]).

The aforementioned individual aerodynamic and structural models are incorporated into a globally-convergent trim algorithm based on Broyden's numerical algorithm. The trim algorithm solves for the rotor collective and longitudinal and lateral cyclic controls for given wind tunnel conditions and rotor thrust C_T , rolling C_L and pitching moment C_M coefficients.

2.2. Rotor aeroacoustics model

The noise prediction code ICARUS (Integral Computational AeRoacoustics Unified Software), is deployed to model helicopter rotor aeroacoustics (Ref. [19]). This code is an integral implementation of the Ffowcs Williams-Hawkings (FW-H) equation (Ref. [20]), which is the most general form of Lighthill's Acoustic Analogy (Ref. [21]). The FW-H equation describes acoustic pressure disturbances as a three-dimensional mechanical wave, equal to three noise source terms, which are monopole, dipole and quadrupole sources, respectively.

Formulation 1A of Farassat (Refs. [22], [23]) is the most extensively utilized and validated integral solution of the FW-H equation. It is based on the free-space Green's function solution of the three-dimensional wave equation. Formulation 1A resolves thickness and loading noise components, which correspond to the monopole and dipole acoustic terms, respectively. The high-speed impulsive noise component which corresponds to the quadrupole term of the FW-H equation is neglected. This is valid as long as the rotor tip Mach number is below the transonic limit, which is the typical condition for the majority of civil rotorcraft operations.

Chordwise compact acoustic expressions of Formulation 1A are utilized since the blade chord can be considered small compared to the wavelength of the radiated acoustic content (Ref. [16]). Brentner *et al.* (Ref. [24]) introduced a compact form of the loading noise term of the Formulation 1A, utilizing the blade-element lift distribution \vec{L} across the blade span. Consequently, the computation reduced from a surface integral to a line integral. Lopes (Ref. [25]) presented and validated a compact expression of the monopole term of Formulation 1A, based on the geometrically compact assumption that the radiation distance is large compared to the blade chord. The proposed formulation utilizes the spanwise distribution of the airfoil cross-sectional area A_{cs} as a blade design parameter of each blade element with differential span length dy . Hence, the thickness acoustic pressure is also evaluated as a line integral defined by the line equation $f = 0$, which describes the blade elastic line ranging from the root to the tip. Using the shorthand notation introduced by Lee *et al.* in Ref. [26] and followed by Lopes in Ref. [25], the compact expressions of thickness and loading acoustic pressure employed in this work can be formed as follows:

$$\begin{aligned}
 (4) \quad \frac{4\pi}{\rho_0} p'_m(\vec{x}, t) &= \int_{f=0} A_{cs} \left(W + \frac{\partial W}{\partial \tau} \right) R(2, 4) \Big|_{ret} dy \\
 &+ \int_{f=0} 2A_{cs} W^2 R(3, 5) \Big|_{ret} dy \\
 &- \int_{f=0} c_0 A_{cs} \frac{\partial \vec{M}}{\partial \tau} \cdot \hat{r} R(2, 3) \Big|_{ret} dy \\
 (5) \quad 4\pi c_0 p'_d(\vec{x}, t) &= \int_{f=0} \frac{\partial \vec{L}}{\partial \tau} \cdot \hat{r} R(1, 2) \Big|_{ret} dy \\
 &+ \int_{f=0} c_0 \left(\vec{L} \cdot \hat{r} - \vec{L} \cdot \vec{M} \right) R(2, 2) \Big|_{ret} dy \\
 &+ \int_{f=0} \vec{L} \cdot \hat{r} W R(2, 3) \Big|_{ret} dy
 \end{aligned}$$

where p'_m and p'_d are the monopole and dipole acoustic disturbance terms respectively, evaluated at the observer position \vec{x} and observer time t and c_0 and ρ_0 are the speed of sound and density of the

quiescent acoustic medium, respectively. The vectors \vec{L} , \vec{M} and \hat{r} correspond to the loading vector, the local relative Mach number vector and the unit radiation vector, respectively. It is noted that the time derivatives are being evaluated in the source time τ . The subscript "ret" represents numerical integration within the retarded-time (i.e. source-time). The following shorthand functions are being used, as suggested by Lopes (Ref. [25]):

$$(6) \quad R(n, m) = r^{-n} (1 - \vec{M} \cdot \hat{r})^{-m}$$

$$(7) \quad W = r \frac{\partial \vec{M}}{\partial \tau} \cdot \hat{r} + c_0 \left(\vec{M} \cdot \hat{r} - |\vec{M}|^2 \right)$$

The source-time-derivative of the function W has been analytically determined by Lee (Ref. [26]):

$$\begin{aligned}
 (8) \quad \frac{\partial W}{\partial \tau} &= r \frac{\partial^2 \vec{M}}{\partial \tau^2} \cdot \hat{r} - 3c_0 \frac{\partial \vec{M}}{\partial \tau} \cdot \vec{M} + \\
 &+ \frac{c_0}{r} \left(r \frac{\partial \vec{M}}{\partial \tau} \cdot \hat{r} + c_0 \left(\left(\frac{\partial \vec{M}}{\partial \tau} \cdot \hat{r} \right)^2 - |\vec{M}|^2 \right) \right)
 \end{aligned}$$

where r is the radiation distance and $|\vec{M}|$ is the magnitude of the local relative Mach number vector.

The overall discrete frequency acoustic pressure $p'(\vec{x}, t)$ can be expressed as the summation of monopole and dipole acoustic disturbance contributions. The compact acoustic formulations adopted in this study are compatible with the lifting-line-type aerodynamic input provided by the free-wake airloads model. Moreover, computational savings of up to 99.5% have been reported with only slight deviations from the corresponding non-compact deterministic acoustic pressure computations (Refs. [24], [25]).

2.3. Uncertainty quantification method

Traditional approaches for uncertainty analysis involve Monte Carlo (MC) simulation which is based on random sampling of the uncertain input parameters. Subsequently, deterministic evaluations of the investigated model are performed for each sample point and the output quantities of interest statistically examined. MC methods are widely used due to the ease of implementation, but the number of samples required for convergence of the statistical properties of the outputs is typically in the order of thousands of evaluations (Refs. [27], [28]). This number becomes prohibitive when the deterministic model evaluations are computationally demanding.

Stochastic spectral methods constitute an efficient alternative to the computationally expensive MC-based methods for uncertainty quantification (UQ). PCE has been utilized for the quantification of uncertainty in aeroacoustics when the deterministic model is computationally demanding (Refs. [5]–[7]). A PCE approach (Ref. [29]) is employed for the quantification of uncertainty in aeroacoustic analysis due to the uncertainty in wake tip-vortex core physical

parameters utilized in this work. PCE describes the response $Y(\xi)$ of a system encompassing stochastic input of known distribution ξ as an infinite series of orthogonal polynomial basis functions $\varphi_i(\xi)$, provided that the response behavior is smooth. For practical engineering applications, the infinite series is truncated to a number of $p+1$ basis functions. Hence:

$$(9) \quad Y(\xi) = \sum_{i=0}^p \varphi_i(\xi) a_i$$

where a_i are the coefficients of the orthogonal polynomial basis functions. The orthogonal polynomials basis functions $\varphi_i(\xi)$ are solely specified by the known random distribution ξ , hence no input from the deterministic model is yet required. Therefore, the estimation of the stochastic response of the system, according to Eq. 9, requires only the determination of the coefficients a_i of the polynomial terms. These are determined by solving the linear system of equations formed by the expansion of Eq. 9:

$$(10) \quad \begin{bmatrix} y(\xi_0) \\ \vdots \\ y(\xi_m) \end{bmatrix} = \begin{bmatrix} \varphi_p(\xi_0) & \cdots & \varphi_0(\xi_0) \\ \vdots & \ddots & \vdots \\ \varphi_p(\xi_m) & \cdots & \varphi_0(\xi_m) \end{bmatrix} \begin{bmatrix} a_p \\ \vdots \\ a_0 \end{bmatrix}$$

where ξ_i are the $m+1$ collocation points at which the system's deterministic response is evaluated, $y(\xi_i)$ is the response of the system at each collocation point and a_i the unknown coefficients of the polynomial of order p . The number of collocation points, which corresponds to the number of deterministic evaluations of the system with n uncertain input parameters, is the cardinality of the dataset \mathcal{E} and is given by:

$$(11) \quad \text{card}(\mathcal{E}) = 1 + \sum_{i=1}^p \frac{1}{i!} \prod_{j=0}^{i-1} (n+j) = \frac{(n+p)!}{n!p!}$$

The low-discrepancy Halton sequence is employed for the determination of collocation points, which offers better coverage of the stochastic space compared to random sampling methods (Ref. [30]). Typically, over-sampling is required to improve the accuracy of the system's response approximation with PCE (Ref. [30]). The effective polynomial expansion is finally derived through least-squares regression (Ref. [31]). PCE treats the deterministic model as a black-box; hence it is a non-intrusive method for uncertainty quantification, which is a suitable approach for engineering applications.

Orthogonal polynomials are based on the probability density function of the random parameters; hence they feature convenient properties for statistical analysis. According to Ref. [32] the mean and variance of the system's output can be analytically derived from the polynomial basis functions and corresponding coefficients. However, for the purposes of this study the developed PCE-based approximation will be used as a

meta-model to be provided to a MC analysis method. Apart from computing statistical moments, this can provide an extensive, but now computationally affordable stochastic dataset for detailed statistical analysis. Additionally, PCE enables the capability of directly performing variance-based sensitivity analysis to identify the relative sensitivity of the stochastic output to the uncertain input parameters. Sensitivity analysis based on Sobol indices S_i (Refs. [33], [34]) is allowed when the response of the system can be decomposed in summands that are mutually orthogonal.

A comprehensive statistical method based on the aforementioned approach has been developed for the purposes of this work. An overview of the integrated statistical method is presented in Fig. 1.

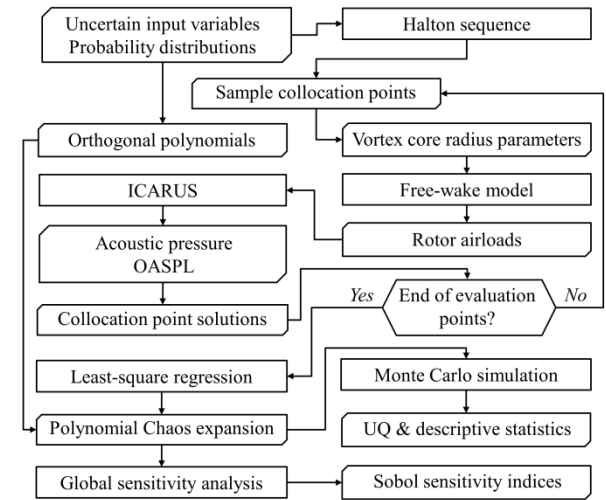


Fig. 1: Overview of uncertainty quantification method.

3. RESULTS AND DISCUSSION

3.1. Comparison with experimental measurements

The accuracy and validity of the developed aeroacoustic simulation method is assessed through comparing predictions with experimental measurements retrieved from the baseline case of the HART II experiment (Ref. [9]). The rotor is a 40% scale model of the 4-bladed hingeless Bo 105 helicopter rotor. The rotor radius is $R = 2 \text{ m}$ and the rotational speed is $\Omega = 109.12 \text{ rad/s}$. The rotor is descending with a shaft angle $\alpha_s = -4.5 \text{ deg}$, advance ratio $\mu = 0.15$ and thrust coefficient $C_T = 0.0044$. Fig. 2 (a) illustrates the comparison of predicted and measured acoustic pressure history at the advancing side observer located 2.215 m below the rotor disc, 0.0 m upstream and 1.81 m at the advancing side of the rotor. It is shown that the developed method accurately predicts the generated BVI noise in terms of amplitude and phase.

A spectral comparison of the acoustic pressure time histories is required to thoroughly quantify the predictive accuracy of the aeroacoustic formulation. Fig. 2 (b) presents the spectral content of the predicted acoustic signal, compared with the corresponding noise results of the measured acoustic history for the first 40 harmonics of the Blade Passage Frequency (BPF),

where BVI noise dominates (Ref. [9]). It is observed that the measured acoustic signal is not entirely periodic due to the additional pressure sensors installed on Blade 1, which caused flapping and loading discrepancies relative to Blades 2-4 (Ref. [9]). For this reason, each of the pulses of the measured signal has been individually analyzed.

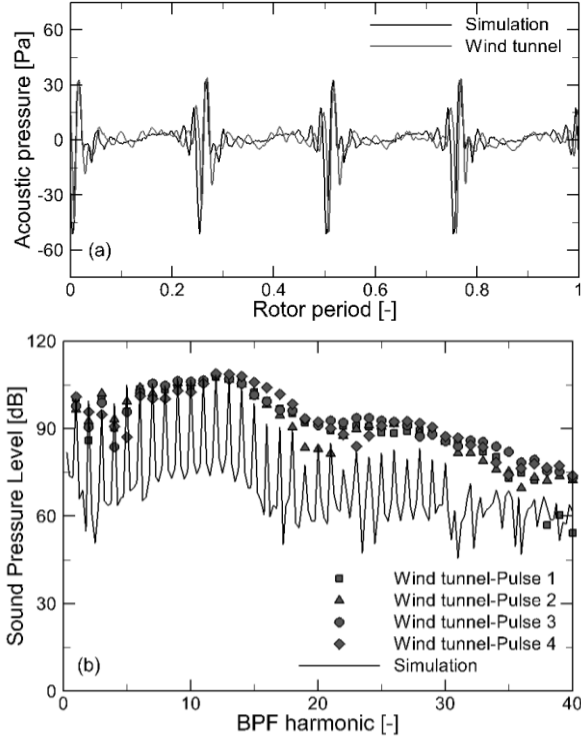


Fig. 2: Acoustic pressure prediction for the HART II rotor – comparison with experimental data from Ref. [9]: (a) acoustic pressure history; (b) spectral analysis.

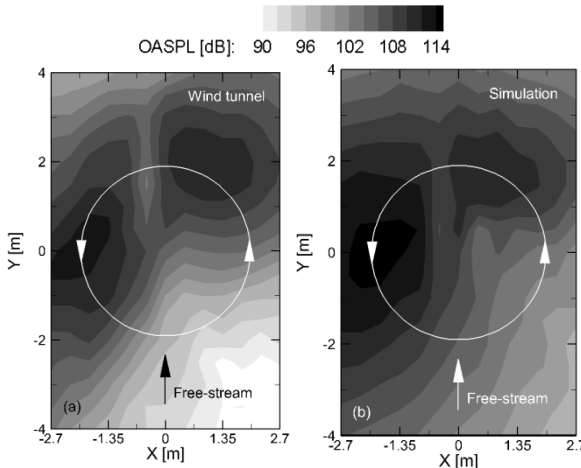


Fig. 3: Ground noise prediction for the HART II rotor – comparison with experimental data from Ref. [9]: (a) wind tunnel; (b) simulation.

As regards the low-frequency content of the noise signal, good agreement between predictions and measurements is observed for the first five BPF harmonics, albeit with discrepancies associated with the 4th and 5th harmonic. These can be attributed to the deviations observed around the second negative peak

of each acoustic pulse and especially in pulses 3 and 4. As regards the higher-frequency BVI content, good agreement is observed up to the 30th BPF harmonic, with a mean relative error of 6.54%. Higher discrepancies are recorded at the higher harmonics which showcase the limitations of chordwise compact aerodynamic and aeroacoustic formulations. Nevertheless, the amplitude of higher harmonic noise components is significantly smaller.

Fig. 3 (a) illustrates the ground noise contours corresponding to the BL case of the HART II experiment. The measurement plane is located 2.215 m below the rotor disc. The OASPL were calculated via frequency-integration of the Fast Fourier Transformation (FFT) on the original acoustic pressure signal at microphone location. Only BPF harmonics between the 6th and the 40th were considered to isolate the mid-frequency content of the emitted noise, where BVI noise is dominant. **Fig. 3 (b)** presents the predicted ground noise for the same conditions using the developed computational models. It can be seen that the advancing and retreating side BVI peaks are accurately predicted in terms of directivity and intensity. An average absolute deviation of 4.1 dB was calculated, which can be deemed as satisfactory given the complexity of the simulated case. It is noted that the experimental scatter of the noise radiation was found to be up to 2 dB (Ref. [9]).

3.2. Polynomial Chaos expansion

The uncertain input parameters considered in this work are the tip-vortex core radius model governing parameters, r_{c0}^{wake} , a_1^{wake} , r_{c0}^{inflow} and a_1^{inflow} . Two distinct cases of input uncertainty are examined: (a) the case when experimental data referring to tip vortex core geometry are available and (b) the case of absent experimental data. For the case of available experimental data, the probability density function (PDF) of all input parameters will be considered to be Gaussian with coefficient of variation $COV = 10\%$. This is in correspondence with experimental measurements of tip-vortex core radius and circulation strength undertaken by Bhagwat and Ramasamy (Ref. [8]). The associated values of mean μ and standard deviation σ of the uncertain inputs considered are summarized in Table 1.

Table 1: Distributions of uncertain input variables when experimental data are available (Gaussian distribution with $COV = 10\%$).

Uncertain input	μ	σ	Unit
r_{c0}^{wake}	0.10	0.01	[chords]
a_1^{wake}	0.001	0.0001	[-]
r_{c0}^{inflow}	0.60	0.06	[chords]
a_1^{inflow}	0.008	0.0008	[-]

As regards the case of absent experimental data for tip-vortex core radius calibration, a uniform distribution is used for all uncertain inputs, as they can

take any value within the designated limits, with equal probability of occurrence. The determination of the upper limit a and lower limit b for each uncertain input is dependent upon the availability of relevant literature and practical experience. Based on the suggestions of Ref. [18] and Ref. [9], as well as the discussion of Section 2.1, an uncertainty of $COV = 30\%$ will be adopted for this investigation, which can be considered as a relatively conservative choice. The resulting limits of the uniform distribution of each uncertain input variable are provided in Table 2. It is noted that in both examined cases, the mean values of uncertain inputs correspond to the values found that provide the best agreement between predicted and experimental noise data, as validated in Section 3.1.

Table 2: Distributions of uncertain input variables when experimental data are not available (Uniform distribution with $COV = 30\%$).

Uncertain input	a	b	Unit
r_{c0}^{wake}	0.0480	0.1519	[chords]
a_I^{wake}	0.00048	0.00152	[-]
r_{c0}^{inflow}	0.2882	0.9117	[chords]
a_I^{inflow}	0.00384	0.01215	[-]

Fig. 4 presents the probability distributions of the r_{c0}^{wake} uncertain input for the two examined cases. The rest of uncertain input parameters are stochastically described by similarly shaped distributions. It is noted that for the case of availability of experimental evidence, the COV values reported in Ref. [8] do not exactly match at 10%. However, due to the fundamental character of this study, it has been deemed as more easily interpretable to maintain a common COV for each uncertain variable, thus allowing the expansion and generalization of obtained results, as will be described in Section 3.6.

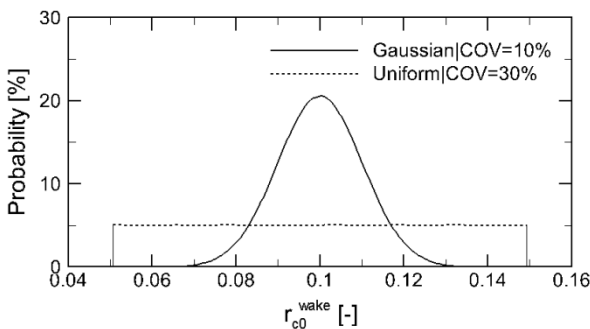


Fig. 4: Comparison of probability density functions for the distribution of r_{c0}^{wake} referring to the two examined cases of input uncertainty.

The stochastic space is discretized based on the sampling method described in Section 2.3. An over-sampling coefficient of 4 is used in this work to generate a reliable sample. A polynomial order $p = 2$ is selected in this work, as also followed in Ref. [7].

Based on Eq. 11 and for the given number of uncertain inputs $n = 4$, a total of 60 collocation points are required for the PCE. The coupled approach comprising free-wake aerodynamics and ICARUS aeroacoustics is employed for the evaluation of each collocation point, as shown in Fig. 1. The output objectives of interest constitute aerodynamic and aeroacoustic descriptors of parameters which govern BVI noise generation and propagation. Specifically, the objectives chosen for UQ are: (a) amplitude of time-derivative of normal force coefficient at $0.87R$ on the advancing side of the rotor

$(dC_n M^2 / d\psi)_{amp}^{adv}$, (b) amplitude of time-derivative of normal force coefficient at $0.87R$ on the retreating side of the rotor $(dC_n M^2 / d\psi)_{amp}^{ret}$, (c) amplitude of acoustic pressure signal at the advancing-side microphone p'_{amp}^{adv} , (d) amplitude of acoustic pressure signal at the retreating-side microphone p'_{amp}^{ret} , (e) overall noise levels at the advancing-side microphone $OASPL^{adv}$ and (f) overall noise levels at the retreating-side microphone $OASPL^{ret}$. The microphone positions considered are the ones reported in Ref. [9].

Before commencing the UQ process, the predictive accuracy of the derived PCE is assessed through Leave-One-Out Cross-Validation (LOOCV). The leave-one-out method is based on the construction of a dedicated PCE at each collocation point after excluding this specific point from the dataset. Then, the PCE-predicted value of the objective functions at this sample point is compared with the corresponding value obtained from the direct evaluation of this point using the actual simulation model. The aforementioned process is repeated for the entire set of sample points of the PCE procedure. The quality of the original PCE is assessed in terms of Pearson's product moment of correlation $N_{Pearson}$ along with the gradient of the associated linear regression line (Ref. [35]). A perfectly linear correlation would correspond to $N_{Pearson} = 1.00$ and a regression line gradient of 45.00 deg.

Table 3: Statistics of LOOCV of the derived PCE when experimental data are available (Gaussian distribution with $COV = 10\%$).

Objective	$N_{Pearson}$ [-]	Grad [deg]	NRMSE [%]	σ [%]
$(dC_n M^2 / d\psi)_{amp}^{adv}$	0.999	45.05	0.469	0.473
$(dC_n M^2 / d\psi)_{amp}^{ret}$	0.995	44.55	1.004	1.011
p'_{amp}^{adv}	0.998	44.68	0.649	0.632
p'_{amp}^{ret}	0.996	45.34	0.977	0.963
$OASPL^{adv}$	0.999	45.01	0.109	0.110
$OASPL^{ret}$	0.996	44.76	0.161	0.169

Table 3 summarizes the statistical properties of LOOCV for all objectives corresponding to the case of known experimental data for tip vortex core calibration. Excellent linear correlation is observed for all objectives, with $N_{Pearson}$ and gradients very close to the ideal values. This showcases the ability of the developed PCE to replicate the physical behavior of the direct simulation. Furthermore, the normalized root-mean-square error (NRMSE) of each objective is lower than 1.004% which quantified the predictive accuracy of the developed PCE. Finally, the corresponding standard deviation σ of the calculated error is again in the same order for all variables. This indicates that the PCE error is uniformly distributed throughout the investigated design space. As regards the case of absent experimental data with uniformly distributed uncertain inputs with $COV=30\%$, similar trends with the previous case are observed, albeit with slightly higher NRMSE (less than 2%), which is attributed to the wider spread of the vortex-core related input variables. However, higher values of output uncertainty are anticipated in this case, which brings the relative contribution of LOOCV uncertainty to similar levels to the $COV=10\%$ Gaussian case. Summarizing, the quantification of quality and accuracy of the developed PCE confirms the applicability of the method in the context of uncertainty quantification for BVI noise prediction.

3.3. Uncertainty quantification

The derived computationally efficient PCE-based meta-models can now be utilized for UQ in BVI noise prediction subject to tip vortex core radius uncertainty. The quantification of uncertainty is implemented through MC simulation based on results of the PCE meta-model. **Table 4** provides the results of UQ for the case when vortex-core experimental data are available (Gaussian distribution with $COV=10\%$).

Table 4: Uncertainty quantification when experimental data are available (Gaussian distribution with $COV=10\%$).

Objective [unit]	μ [unit]	σ [unit]	γ_1 [-]	γ_2 [-]
$(dC_n M^2 / d\psi)_{amp}^{adv} / \frac{1}{rad}$	0.82	0.12	0.424	0.112
$(dC_n M^2 / d\psi)_{amp}^{ret} / \frac{1}{rad}$	0.62	0.07	0.608	0.364
$p'_{amp}^{adv} [Pa]$	84.12	9.91	0.327	0.046
$p'_{amp}^{ret} [Pa]$	46.64	5.56	0.318	0.024
$OASPL^{adv} [dB]$	114.4	1.17	0.013	-0.113
$OASPL^{ret} [dB]$	111.1	1.14	0.027	-0.064

It is observed that the mean values of $(dC_n M^2 / d\psi)_{amp}^{adv}$ and $(dC_n M^2 / d\psi)_{amp}^{ret}$ are identical to the deterministic simulation results, whilst the corresponding uncertainties reach 15.35% and 11.90%

of the associated mean values, respectively. As regards p'_{amp}^{adv} and p'_{amp}^{ret} , the stochastic mean values are slightly higher than the corresponding deterministic amplitudes (0.36% and 0.88%), with associated uncertainties of 11.78% and 11.93%, respectively. The stochastic prediction of mean $OASPL^{adv}$ and $OASPL^{ret}$ is almost identical to the corresponding deterministic noise values. The associated uncertainty is 1.02% for both microphone locations, which represents a standard deviation of approximately 1.1 dB.

The skewness γ_1 of each objective distribution describes the degree of distortion from the symmetrical “bell-shaped” distribution. It can be seen that for the $COV=10\%$ case with Gaussian input uncertainty distributions, the stochastic output objectives are fairly symmetrical, with values of γ_1 generally below 0.5.

Especially for $OASPL^{adv}$ and $OASPL^{ret}$, skewness is below 0.05 which corresponds to an almost fully-symmetrical distribution. The excess kurtosis γ_2 is a measure of outliers present in the distribution. It is noted that the kurtosis of Gaussian distribution is 3 by definition. Hence, a value of $\gamma_2=0$ would represent a perfectly Gaussian distribution. It is shown that for the $COV=10\%$ case with Gaussian input uncertainty the stochastic output objectives follow distributions close to mesokurtic, with values of γ_2 generally below 0.5. Overall, it can be concluded that in cases when experimental data referring to the tip vortex core radius are available, fairly robust aeroacoustic predictions can be made, which confirms the suitability of free-wake/FW-H approaches in the context of complex BVI noise prediction.

Table 5: Uncertainty quantification when experimental data are not available (Uniform distribution with $COV=30\%$).

Objective [unit]	μ [unit]	σ [unit]	γ_1 [-]	γ_2 [-]
$(dC_n M^2 / d\psi)_{amp}^{adv} / \frac{1}{rad}$	0.87	0.28	0.946	-0.037
$(dC_n M^2 / d\psi)_{amp}^{ret} / \frac{1}{rad}$	0.67	0.18	0.841	-0.008
$p'_{amp}^{adv} [Pa]$	86.96	21.74	0.704	-0.267
$p'_{amp}^{ret} [Pa]$	48.37	12.43	0.782	-0.074
$OASPL^{adv} [dB]$	114.6	3.71	0.024	-0.705
$OASPL^{ret} [dB]$	111.2	3.32	0.061	-0.618

Table 5 presents the uncertainty analysis for the case of absent experimental evidence regarding tip vortex core radius, essentially described by uniformly distributed uncertain input variables with $COV=30\%$. Trends similar to **Table 4** are observed, albeit with higher levels of uncertainty. Specifically, the uncertainty

in p'_{amp}^{adv} and p'_{amp}^{ret} prediction is approximately 25% for both microphone locations, whilst the associated stochastic mean values are 3.75% and 12.84% higher than the corresponding deterministic predictions. Standard deviations of 3.71 dB and 3.32 dB are calculated for the $OASPL^{adv}$ and $OASPL^{ret}$ objectives, respectively, although these retain stochastic mean predictions almost identical to the deterministic ones.

Furthermore, the distributions of $(dC_n M^2 / d\psi)_{amp}$ and p'_{amp} are moderately skewed to the right with γ_1 reaching positive values of almost 1. In this case, the mean value of output objectives is significantly higher than the mode of the distributions, which is the objective value with the highest probability of occurrence. Hence, by neglecting the input uncertainty in this case, the most probable output would be an under-estimated descriptor of unsteady airloads or acoustic pressure. Nevertheless, the symmetry of OASPL is retained at even high values of input uncertainty. However, the associated excess kurtosis is considerably negative, with values lower than -0.5, which is primarily attributed to the uniform distribution of input uncertainty.

3.4. Sensitivity analysis

The relative contribution of individual uncertain inputs to the overall stochastic response is quantified through sensitivity analysis based on Sobol indices, as described in Section 3.3. Table 6 presents the sensitivity indices S_i referring to the case of available tip-vortex data with Gaussian $COV = 10\%$.

Table 6: Sensitivity of output objectives to uncertain inputs when experimental data are available (Gaussian distribution with $COV = 10\%$).

Objective	Sensitivity index S_i [%]			
	r_{c0}^{wake}	a_1^{wake}	r_{c0}^{inflow}	a_1^{inflow}
$(dC_n M^2 / d\psi)_{amp}^{adv}$	0.018	0.009	27.610	72.360
$(dC_n M^2 / d\psi)_{amp}^{ret}$	0.263	0.029	35.511	64.195
p'_{amp}^{adv}	0.010	0.015	27.383	72.590
p'_{amp}^{ret}	0.037	0.004	46.923	53.034
$OASPL^{adv}$	0.002	0.013	27.755	72.228
$OASPL^{ret}$	0.023	0.003	47.171	52.801

It is observed that uncertainty in the parameters used for wake geometry calculations, r_{c0}^{wake} and a_1^{wake} , has insignificant influence on aeroacoustic outputs. However, inflow-related input uncertainty and especially uncertainty in the value of Squire parameter

a_1^{inflow} has approximately 72% contribution to the overall system's response. It is noted that similar trends have been observed in the sensitivity analysis of the $COV = 30\%$ case with uniform input distributions, which illustrates that the relative contribution of input parameters is not dependent upon the shape and value of input uncertainty.

Additionally, it is observed that the sensitivity indices of a_1^{inflow} are consistently higher at the advancing side, compared with the corresponding indices of retreating side. This is attributed to the tip vortex behavior at both sides of the rotor. As shown in Refs. [9], [10], retreating rotor blades interact with trailed tip vortices of age less than 90 deg. At the early stages of tip vortex propagation, vortex core growth is minimal, which in combination with a small r_{c0} can lead to small vortex core radii which directly affect induced velocity and airloads. A larger r_{c0} would act as a "damper" of excessively high vortex core radii. This highlights the importance of the initial vortex core radius parameter in UQ of retreating-side BVI noise. As regards advancing-side BVIs, most of interactions comprise relatively older tip vortex filaments with an age greater than 90 deg., hence the impact of r_{c0}^{inflow} is reduced relative to the retreating-side BVI uncertainty.

3.5. Stochastic aeroacoustic predictions

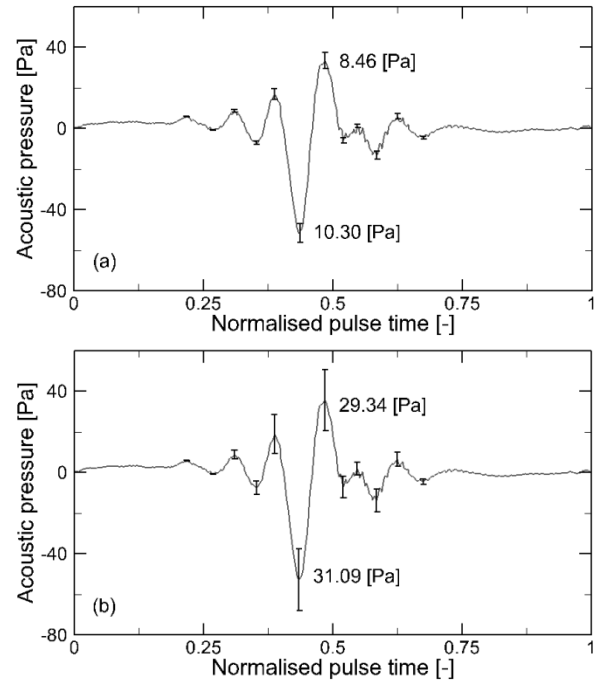


Fig. 5: Stochastic prediction of acoustic pressure at the HART II advancing side observer – mean acoustic pressure and uncertainty bars representing two standard deviations: (a) Gaussian input with $COV = 10\%$; (b) Uniform input with $COV = 30\%$.

Fig. 5 (a) presents the stochastic prediction of full time-history of a single BVI acoustic pressure pulse

for the case of Gaussian $COV = 10\%$ input distribution of the tip vortex core parameters. The acoustic pressure time-histories of all sample collocation points have been aligned together to remove any phase shift between the 60 acoustic signals. The illustrated acoustic pressure distribution represents the mean p^{adv} value at each point of the time-history. The distribution of stochastic mean acoustic pressure is almost identical to the deterministic predictions illustrated in **Fig. 2 (a)**. Superimposed are the uncertainty bars representing two standard deviations of p^{adv} at each time-point. It can be seen that a standard deviation of 4.23 Pa corresponds to the positive peak of BVI pulse, whilst a 5.15 Pa uncertainty is recorded at the negative peak. The resulting stochastic amplitude of acoustic pressure is very close to the $p_{amp}^{adv} = 9.91 Pa$ calculated in

Section 3.3, which confirms the suitability of the employed descriptor as objective of the UQ process.

Fig. 5 (b) presents the corresponding stochastic prediction for uniform input distributions of $COV = 30\%$. The mean stochastic acoustic pressure distribution is similar to the deterministic, although slightly over-predicted, with peak local differences reaching 2.1%. The width of uncertainty bars follows same trends as in the Gaussian $COV = 10\%$ case, however, the maximum uncertainties reach 14.67 Pa and 15.55 Pa at the positive and negative peaks of the BVI pulse, respectively.

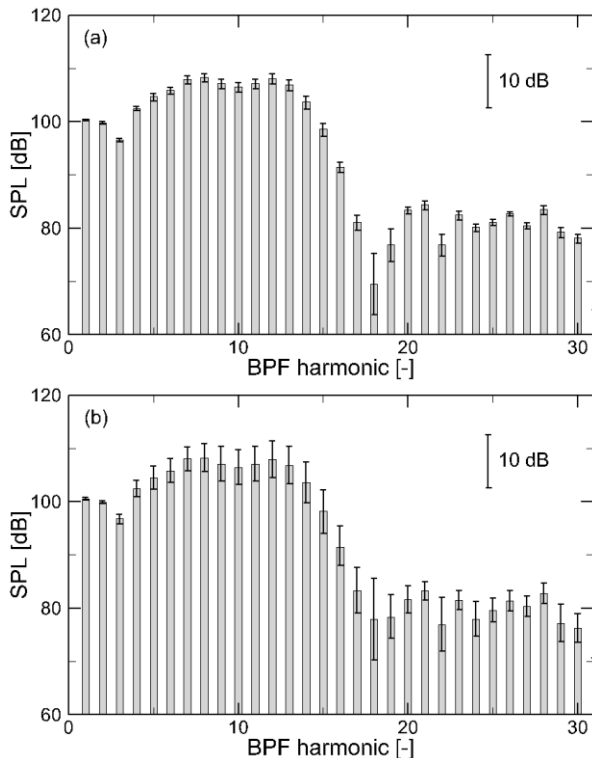


Fig. 6: Stochastic prediction of spectral content at the advancing side observer of the HART II experiment – mean SPL and uncertainty bars representing two standard deviations: (a) Gaussian input with $COV = 10\%$; (b) Uniform input with $COV = 30\%$.

The distribution of uncertainty in the time-domain stochastic prediction of acoustic pressure is reflected in the spectral analysis in the frequency range where BVI noise is dominant. **Fig. 6 (a)** and **Fig. 6 (b)** illustrate the mean Sound Pressure Levels (SPL) with superimposed uncertainty bars corresponding to the $COV = 10\%$ and $COV = 30\%$ cases, respectively. The stochastic mean values are identical across the entire frequency range, which confirms the immunity of mean SPL to vortex core input uncertainties. For the case of Gaussian input with $COV = 10\%$, relatively small levels of uncertainty are observed across the entire frequency range, with standard deviations in the order of 1 dB. This highlights the robustness of free-wake/FW-H approaches in predicting BVI noise when experimental data referring to tip vortex core growth are available. However, in the case without this data, uncertainties in the order of 3.5 dB govern the mid-frequency content, corresponding to the BVI signal, which can primarily be attributed to the high standard deviations observed around the peaks of the acoustic pressure pulse. It is noted that the low-frequency harmonic noise is less affected by vortex-core-related uncertainty, as standard deviations below 1 dB are associated with the first three BPF harmonics.

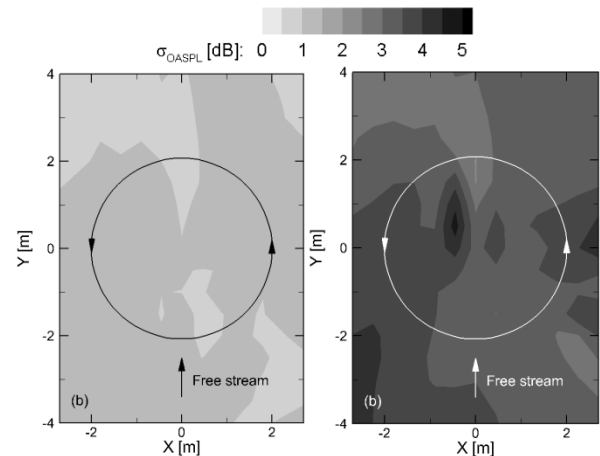


Fig. 7: Standard deviation of stochastic prediction of ground noise 2.215 m below the HART II rotor: (a) Gaussian input with $COV = 10\%$; (b) Uniform input with $COV = 30\%$.

The impact of uncertainty in the BVI ground noise predictions is illustrated in **Fig. 7 (a)** and **Fig. 7 (b)**, which present the distribution of standard deviation in dB for the stochastic prediction of 6-40 BPF mean ground noise distribution of the HART II experiment (**Ref. [9]**). It is noted that the mean OASPL distribution is very similar to the deterministic presented in **Fig. 3 (b)**, hence it was deemed sufficient to only present the corresponding standard deviations. Generally, the prediction of ground noise contour is adequately robust in the $COV = 10\%$ case, with values of standard deviations not exceeding 1 dB at most measurement nodes. As regards the uniform-input $COV = 30\%$ case, uncertainty can reach up to 4.6 dB, dictating the importance of stochastic simulation when experimental evidence referring to the vortex core geometry is not available.

3.6. Fundamental modeling guidelines

The previous analysis has shown that the impact of input uncertainty on the robustness of aeroacoustic predictions is dependent upon the shape and COV of input distributions.

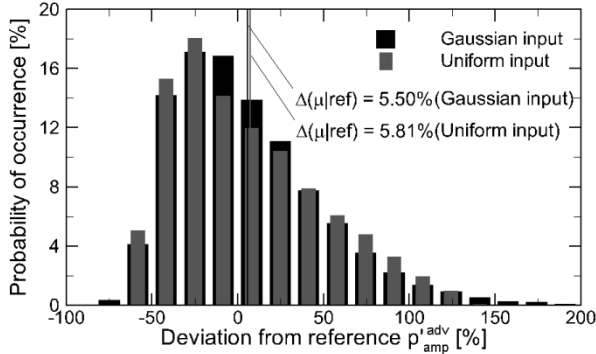


Fig. 8: Probability histograms for Gaussian and uniform input uncertainty of $COV = 30\%$.

Fig. 8 presents the probability histograms of p_{amp}^{adv} , comparing the cases of Gaussian and uniform uncertain input distributions, both with $COV = 30\%$. The distributions are expressed as relative deviation from the p_{amp}^{adv} which achieves the best match with experimental data, as presented in **Fig. 2 (a)**. This value will be used as reference for the entire analysis presented in this section. It can be seen that both distributions are positively skewed with modes Mo around -25% of the reference value. This depicts the importance of stochastic simulation at high values of input uncertainty: a considerable under-prediction of p_{amp}^{adv} will most probably occur if the case is approached deterministically. On the other hand, stochastic simulation would result to an over-prediction of only 5.8% relative to the reference p_{amp}^{adv} .

The uncertainty quantification method described in **Section 2.3** is repeated for a wide range of input COV and for two different shapes of input distributions, Gaussian and uniform. The outcome of this process is a set of generalized uncertainty maps which can serve as modeling guidelines for analysts. **Fig. 9 (a)** and **Fig. 9 (b)** illustrate the uncertainty map referring to p_{amp}^{adv} for input COV ranging from 0% to 55% and for Gaussian and uniform input distributions, respectively. Each point of the map essentially represents the outputs of full UQ based on dedicated PCEs comprising 60 collocation points each, resulting in a total of 1320 deterministic simulations.

The output p_{amp}^{adv} predictions are provided as percentage changes relative to the reference p_{amp}^{adv} , whilst output uncertainty is presented as percentage of the reference p_{amp}^{adv} . It can be seen that output uncertainty is almost linearly correlated with input uncertainty, with a gradient of approximately 58 deg. for

both distributions. As regards the relative deviation of stochastic mean p_{amp}^{adv} , it is described by a 2nd order polynomial trend, with values generally higher than the reference. The relative deviation of the Mo of p_{amp}^{adv} presents a diverging trend, leading to significant under-predictions at COV greater than 15%. This is the point where input uncertainty starts to become important for the accuracy of acoustic pressure predictions. The difference between the curves corresponding to μ and Mo of the acoustic pressure amplitude predictions essentially quantifies the benefits that arise from stochastic simulation relative to the most probable outcome of the corresponding deterministic execution.

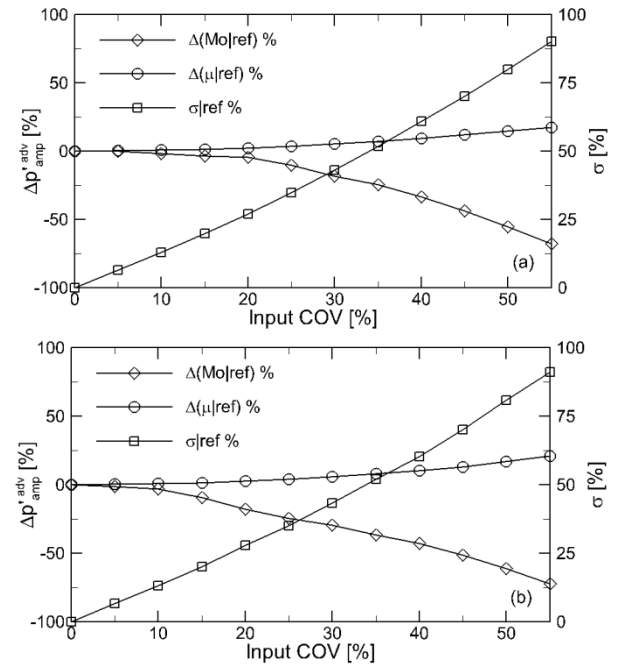


Fig. 9: Impact of input uncertainty on the prediction of acoustic pressure: (a) Gaussian; (b) Uniform input.

Fig. 10 (a) and **Fig. 10 (b)** present the same analysis for the $OASPL^{adv}$ output objective. The stochastic mean-value discrepancies from the reference $OASPL^{adv}$, as well as standard deviation are provided in dB. Generally low deviations of the stochastic mean from the reference are observed, with values not exceeding 1 dB even at high levels of input uncertainty. The associated output uncertainty is again linearly correlated with input COV, with a gradient of 6.4 deg. The relative deviation of the Mo of $OASPL^{adv}$ presents again a diverging trend, with under-predictions of approximately 2 dB at excessively high values of input uncertainty.

Summarizing, for given requirements in terms of accuracy and robustness, the analyst can resort to the developed uncertainty maps in order to: (a) estimate the anticipated error of deterministic simulation (b) evaluate the necessity of stochastic simulation and assess the expected improvement in accuracy, and (c) quantify the associated uncertainty depending on output

objectives and analysis requirements. The above guidelines are applicable for both detailed acoustic pressure prediction and holistic ground noise evaluation referring to helicopter rotors in BVI-dominated flight conditions.

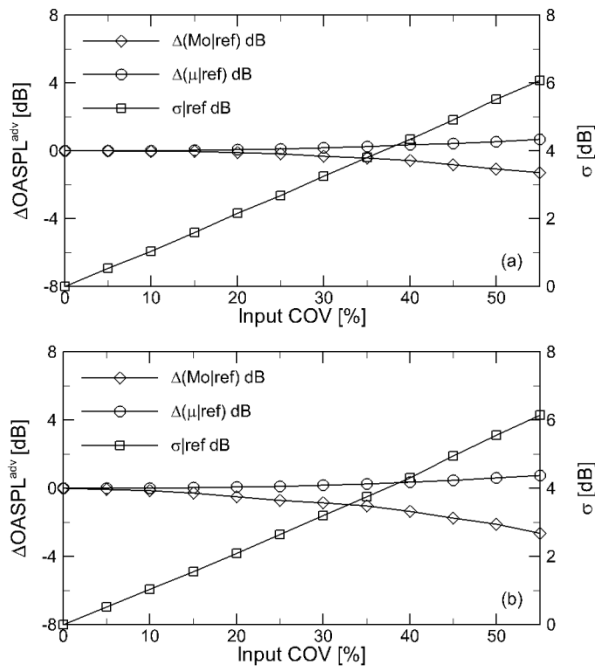


Fig. 10: Impact of input uncertainty on the prediction of OASPL: (a) Gaussian; (b) Uniform input.

4. CONCLUSIONS

A holistic uncertainty analysis has been undertaken, examining the impact of tip vortex core modeling uncertainty on the aeroacoustic simulation of helicopter rotors in BVI conditions. A thorough validation study of the employed free-wake/FW-H solver against the benchmark HART II case depicted the excellent noise predictive accuracy of this method when robust experimental data for the calibration of tip-vortex core model are available. However, considerable uncertainty may be induced to the aeroacoustic predictions when such data are not available.

Two distinct cases have been defined for uncertainty analysis: (a) when experimental data about the geometry of tip vortex core are available and (b) when experimental data are absent. For both cases uncertainty quantification was conducted based on Polynomial Chaos expansion. The quality of the approximation was assessed through Leave-One-Out Cross-Validation, demonstrating the excellent predictive accuracy of the Polynomial expansion and its suitability for uncertainty quantification of highly complex BVI noise cases. The output objectives for statistical analysis were descriptors representative of unsteady rotor airloads, acoustic pressure and OASPL noise.

The BVI acoustic pressure signal is sensitive to even low-levels of input uncertainty. The amplitude of acoustic pressure pulses which effectively determines BVI noise levels, has shown uncertainties around 12% and 25% for the cases of availability and absence of tip-vortex-core experimental evidence, respectively.

A sensitivity analysis based on Sobol indices has been carried out to identify the relative contribution of each uncertain parameter to the overall stochastic response of the system. It was found that the inflow-related parameters, and especially the Squire parameter, have the greatest influence on BVI airloads and noise-related output uncertainty.

It has been shown that in the case of availability of experimental data, the levels of OASPL uncertainty are in the order of 1 dB, which dictates the suitability of free-wake/FW-H approaches as robust tools for modeling helicopter BVI noise. When vortex-core-related experimental data are absent, output uncertainty in the order of 3.5 dB can occur for conservative selection of input uncertainty. This highlights the necessity of stochastic simulation when correlations with tip-vortex experimental data are not feasible.

Furthermore, it has been demonstrated that in the absence of experimental evidence, deterministic approaches could lead to acoustic pressure under-predictions in the order of -25%. For the same case, employment of stochastic simulation improves the accuracy of simulation to values corresponding to only 5.8% over-predictions, relative to the validated reference acoustic pressure.

A generalized set of stochastically derived aeroacoustic predictions, expressed with reference to the validated solution which achieves the best match with experimental data have been provided. The simulations have been carried out at different levels and distributions of input uncertainty, thus providing an uncertainty map which can serve as modeling guidelines for analysts. Specifically, for given requirements in terms of predictive robustness, the analyst can estimate the anticipated error of their deterministic simulation, evaluate the necessity and benefit of stochastic simulation, and quantify the associated levels of uncertainty depending on output objectives and analysis requirements.

ACKNOWLEDGEMENTS

This work has received funding from the Clean Sky 2 Joint Undertaking under the European Union's Horizon 2020 research and innovation programme under grant agreement No. 776900.

The authors would also like to acknowledge Mr. Jos Stevens (NLR), Dr. Gianluigi Alberto Misté (University of Padua), Mr. Nico van Oosten (Anotec Engineering SL) and Mr. Alf Junior (DLR) for their insightful advice on rotorcraft modeling and simulation.

COPYRIGHT STATEMENT

The authors confirm that they, and/or their company or organization, hold copyright on all of the original material included in this paper. The authors also confirm that they have obtained permission, from the copyright holder of any third party material included in this paper, to publish it as part of their paper. The authors confirm that they give permission, or have obtained permission from the copyright holder of this paper, for the publication and distribution of this paper

as part of the ERF proceedings or as individual offprints from the proceedings and for inclusion in a freely accessible web-based repository.

REFERENCES

- [1] M. E. Kelly and R. E. Brown, "The effect of blade aerodynamic modelling on the prediction of the blade airloads and the acoustic signature of the HART II rotor," in *35th European Rotorcraft Forum*, 2009.
- [2] M. Gennaretti, G. Bernardini, J. Serafini, and G. Romani, "Rotorcraft comprehensive code assessment for blade – vortex interaction conditions," *Aerosp. Sci. Technol.*, vol. 80, pp. 232–246, 2018.
- [3] B. Giret, S. Moreau, and J. Boussuge, "Uncertainty quantification of the far-field noise from a rod-airfoil configuration," in *Proceedings of the Summer Program, Center for Turbulence Research, Stanford University, NASA*, 2012, pp. 261–270.
- [4] B. Ivo, F. Nobile, and R. Tempone, "A stochastic collocation method for elliptic partial differential equations with random input data," *SIAM J. Numer. Anal.*, vol. 45, no. 3, pp. 1005–1034, 2007.
- [5] W. F. J. Olsman, "Uncertainty quantification of noise abatement flight procedures," in *41st European Rotorcraft Forum Proceedings*, 2015, p. 32.
- [6] N. Ricks, S. Abraham, F. Contino, and G. Ghorbaniasl, "Sensitivity Analysis and Uncertainty Quantification for the Ffowcs Williams-Hawkins Equation," in *23rd AIAA/CEAS Aeroacoustics Conference*, 2017, p. 3511.
- [7] N. Ricks, S. Abraham, F. Contino, and G. Ghorbaniasl, "Uncertainty quantification for the aeroacoustics of rotating blades in the time domain," *Appl. Acoust.*, vol. 139, no. April, pp. 57–68, 2018.
- [8] M. J. Bhagwat and M. Ramasamy, "Effect of tip vortex aperiodicity on measurement uncertainty," *Exp. Fluids*, vol. 53, no. 5, pp. 1191–1202, 2012.
- [9] B. G. van der Wall, J. W. Lim, J. D. Baeder, and D. D. Boyd, "The HART II international workshop: an assessment of the state-of-the-art in comprehensive code prediction," *CEAS Aeronaut. J.*, vol. 4, no. 3, pp. 223–252, 2013.
- [10] A. Castillo Pardo, "Aeroelastic Simulation of Rotorcraft Propulsion Systems," *Ph.D. thesis, Cranf. Univ. Cranfield, Bedfordshire, UK*, 2017.
- [11] I. Goulos, V. Pachidis, and P. Pilidis, "Lagrangian Formulation for the Rapid Estimation of Helicopter Rotor Blade Vibration Characteristics," *Aeronaut. J.*, vol. 118, no. 1206, pp. 861–901, 2014.
- [12] A. Castillo Pardo, I. Goulos, and V. Pachidis, "Modelling and analysis of coupled flap-lag-torsion vibration characteristics helicopter rotor blades," *Proc. Inst. Mech. Eng. Part G J. Aerosp. Eng.*, vol. 231, no. 10, pp. 1804–1823, 2016.
- [13] I. Goulos, V. Pachidis, and P. Pilidis, "Helicopter Rotor Blade Flexibility Simulation for Aeroelasticity and Flight Dynamics Applications," *J. Am. Helicopter Soc.*, vol. 59, no. 4, pp. 1–18, 2014.
- [14] J. G. Leishman and T. S. Beddoes, "A Semi-Empirical Model for Dynamic Stall," *J. Am. Helicopter Soc.*, vol. 3, pp. 3–17, 1989.
- [15] A. Bagai and J. G. Leishman, "Rotor Free-Wake Modeling Using a Pseudo-Implicit Technique — Including Comparisons with Experimental Data," *J. Am. Helicopter Soc.*, vol. 40, no. 3, pp. 29–41, 1995.
- [16] H. Chen, K. S. Brentner, S. Ananthan, and J. G. Leishman, "A Computational Study of Helicopter Rotor Wakes and Noise Generated During Transient Maneuvers," *J. Am. Helicopter Soc.*, vol. 53, no. 1, pp. 37–55, 2008.
- [17] G. H. Vatistas, V. Kozel, and W. C. Mih, "A simpler model for concentrated vortices," *Exp. Fluids*, vol. 11, no. 1, pp. 73–76, 1991.
- [18] M. J. Bhagwat and J. G. Leishman, "Generalized viscous vortex model for application to free-vortex wake and aeroacoustic calculations," in *American Helicopter Society 58th Annual Forum and Technology Display, Montreal, Canada*, 2002.
- [19] S. Vouros, I. Goulos, and V. Pachidis, "Integrated methodology for the prediction of helicopter rotor noise at mission level," *Aerosp. Sci. Technol.*, vol. 89, pp. 136–149, 2019.
- [20] J. E. Ffowcs Williams and D. L. Hawkins, "Sound Generation by Turbulence and Surfaces in Arbitrary Motion," *Philos. Trans. R. Soc. London. Ser. A, Math. Phys. Sci.*, vol. 264, no. 1151, pp. 321–342, 1969.
- [21] M. J. Lighthill, "On Sound Generated Aerodynamically. I. General Theory," *Proceedings of the Royal Society A: Mathematical, Physical and Engineering Sciences*, vol. 211, no. 1107, pp. 564–587, 1952.
- [22] F. Farassat, "Derivation of Formulations 1 and 1A of Farassat," *NASA/TM-214853*, 2007.
- [23] F. Farassat and G. P. Succi, "The prediction of helicopter rotor discrete frequency noise," in *American Helicopter Society 38th Annual Forum, Washington, DC*, 1982.
- [24] K. S. Brentner, C. L. Burley, and M. A. Marcolini, "Sensitivity of Acoustic Predictions to Variation of Input Parameters," *J. Am.*

Helicopter Soc., vol. 39, no. 3, pp. 43–52, 1994.

- [25] L. V. Lopes, “Compact Assumption Applied to the Monopole Term of Farassat’s Formulations,” *21st AIAA/CEAS Aeroacoustics Conf. AIAA 2015-2673*, pp. 1–22, 2015.
- [26] S. Lee, K. S. Brentner, F. Farassat, and P. J. Morris, “Analytic Formulation and Numerical Implementation of an Acoustic Pressure Gradient Prediction,” *J. Sound Vib.*, vol. 319, no. 3–5, pp. 1200–1221, 2009.
- [27] S. Murugan, R. Ganguli, and D. Harursampath, “Stochastic aeroelastic analysis of composite helicopter rotor,” *J. Am. helicopter Soc.*, vol. 56, no. 1, p. 12001, 2011.
- [28] C. Siva, S. Murugan, and G. Ganguli, “Uncertainty quantification in helicopter performance using Monte Carlo simulations,” *J. Aircr.*, vol. 48, no. 5, pp. 1503–1511, 2011.
- [29] D. Xiu and G. E. M. Karniadakis, “The Wiener--Askey polynomial chaos for stochastic differential equations,” *SIAM J. Sci. Comput.*, vol. 24, no. 2, pp. 619–644, 2002.
- [30] S. Hosder, R. Walters, and M. Balch, “Efficient Sampling for Non-Intrusive Polynomial Chaos Applications with Multiple Uncertain Input Variables,” in *48th AIAA/ASME/ASCE/AHS/ASC Structures, Structural Dynamics, and Materials Conference*, 2007, p. 1939.
- [31] M. Berveiller, B. Sudret, and M. Lemaire, “Stochastic finite element: a non intrusive approach by regression,” *Eur. J. Comput. Mech. Eur. Mécanique Numérique*, vol. 15, no. 1–3, pp. 81–92, 2006.
- [32] K. Wang, G. Li, S. Member, and X. Jiang, “Applying Probabilistic Collocation Method to Power Flow Analysis in Networks with Wind Farms,” in *2013 IEEE Power & Energy Society General Meeting*, 2013, pp. 1–5.
- [33] I. M. Sobol, “Sensitivity Estimates for Nonlinear Mathematical Models,” *Math. Model. Comput. Exp.*, vol. 1, no. 4, pp. 407–414, 1993.
- [34] H. Toshimitsu and A. Saltelli, “Importance measures in global sensitivity analysis of nonlinear models,” *Reliab. Eng. Syst. Saf.*, vol. 52, no. 1, pp. 1–17, 1996.
- [35] I. Goulos and M. Bonesso, “Variable rotor speed and active blade twist for civil rotorcraft: Optimum scheduling, mission analysis, and environmental impact,” *Aerosp. Sci. Technol.*, vol. 1, pp. 1–13, 2019.